Progress In Electromagnetics Research B, Vol. 54, 129–148, 2013

POWER ANGLE SPECTRUM OF SATELLITE COMMUNICATION DOWNLINK IN RAIN ENVIRONMENT AT MILLIMETER-WAVE BANDS

Shu Hong Gong*, Wei Meng, and Jing Yang

School of Science, Xidian University, Box 273, Xi'an 710071, China

Abstract—The study of this paper focuses on the power angle spectrum (PAS) of the satellite communication downlink in rain environment at millimeter-wave bands. The two-dimension angle distribution expression of the incoherent intensity of the ground receiving antenna in rain is deduced in detail. The coherent intensity is discussed according to the first-order multiple scattering approximation theory. The calculation model of PAS is given based on the coherent intensity and the incoherent intensity angle distribution. Based on the Marshall-Palmer raindrop size distribution, the rain-induced attenuation coefficient $\gamma = \rho\langle\sigma_t\rangle$, as well as the average scattering amplitude function of rain area, is calculated and discussed by Mie method; the two-dimension and the one-dimension PASs are simulated and analyzed at different incident angles for different rain rates, frequencies and polarizations. The PAS model and the simulation results given in this paper are important for the quantitative evaluation of the impacts of rain environment on MMW MIMO channel characteristics.

1. INTRODUCTION

With the growing demands for wireless communication, the future communication system needs more advanced technologies to make better use of the limited power, increase the spectrum efficiency and improve the transmission rate and system capacity. In comparison with traditional Single-Input Single-Output (SISO) communication technology, Multiple-Input Multiple-Output (MIMO) technology shows great advantages, such as higher transmission rate, spectrum utilization ratio and power efficiency. Therefore, MIMO

Received 27 July 2013, Accepted 22 August 2013, Scheduled 1 September 2013

* Corresponding author: Shu Hong Gong (ljbrp2003@163.com).

communication technology represents a breakthrough in the modern communication field [1–3].

Many reports about MIMO communication have focused on the frequencies below 10 GHz [1]. In contrast, the research on MMW MIMO communication is still in its infancy, although millimeter wave (MMW) communication technology has many advantages [1]. Available publications just explored some particular aspects for MMW MIMO communication. An overview of MMW MIMO communication system was given in [4]. In [5], it was proposed that MMW MIMO should be used for next generation mobile broadband. The investigation and discussion of MMW MIMO communication in indoor environment was carried out in [6–14]. The short-distance transmission performance of the MMW MIMO system in outdoor clear environment was evaluated and discussed in [15–17]. Some reports explored the antenna of MMW MIMO system [18–20]. The publications of [20–34] studied the channel characteristics, the performance of capacity and BER and the Space-Time Coding of MMW MIMO system, but the influences of the troposphere were not considered. In [35–39], it was particularly pointed out that these effects must be taken into account in order to develop MMW MIMO communication technology.

In addition, attention has been paid to the application of MMW MIMO communication technology in earth-satellite communication system in recent years. For example, MIMO over satellite is reviewed in [2], in which MMW MIMO technology is referred to, preliminary explorations of MMW earth-satellite MIMO communication can be found in [40–43]. Similar to MMW MIMO communication, MMW earth-satellite MIMO communication is still in its infancy. Therefore, futher study on MMW earth-satellite MIMO communication is highly desirable. The evaluation of channel characteristics is important in developing MMW earth-satellite MIMO communication system. Among them, PAS is particularly remarkable because it quantifies the received power of receiving antenna as a function of angle. For example, PAS is needed to evaluate angle spread (AS) characteristic, and it is essential to calculate the channel correlation.

Some models of PAS are given in available publications, such as Cosine distribution [44], Uniform distribution [45], Gaussian distribution [46] and Laplacian distribution [47]. Although these models describe well the power angle distribution caused by terrain and the objects around receiving antenna, such as flat surface ground, hills, mountains, buildings, automobiles, trees, vegetation and so on, they are not suitable for MMW systems. The antenna of MMW communication system has higher gain and narrower beam, and it is usually in line-of-sight state between the ground station and

the satellite antenna for MMW earth-satellite communication system (especially the earth-satellite fixed communication system). Therefore, in contrast to the propagation and scattering effects induced by the troposphere environments, the effects induced by terrain and the objects around receiving antenna seldom impact on MMW channel characteristics. It can be concluded that the PAS models mentioned above are invalid for the earth-satellite MIMO communication system at MMW bands. The scattering and propagation impacts caused by rain represent one of the most challenging problems in MMW communication. To the best of our knowledge, there has been no report on evaluation models of the PAS caused by rain.

This paper focuses on the PAS of the satellite communication downlink in rain environment at millimeter-wave bands. The two-dimension angle distribution expression of the incoherent intensity of the ground receiving antenna in rain is deduced in detail, and the coherent intensity is discussed according to the first-order multiple scattering approximation theory. The calculation model of PAS is given based on the coherent intensity and the incoherent intensity angle distribution. The PAS model and the simulation results given in this paper will be useful for the quantitative evaluation of the impacts of rain environment on MMW MIMO channel characteristics.

2. DERIVATION OF POWER ANGLE SPECTRUM

As shown in Figure 1, the downlink signal passing through a rain area can be regarded as a plane wave incident on a semi-infinite medium containing a random distribution of many raindrops, because

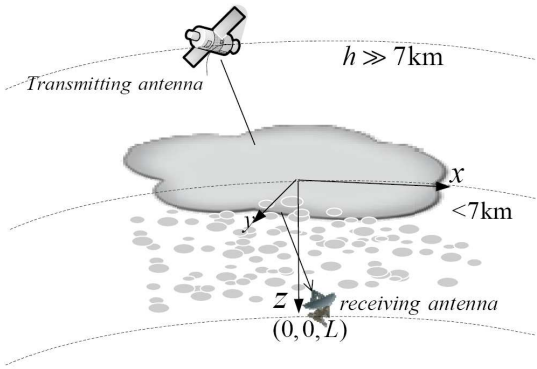

Figure 1. A sketch of the satellite communication downlink in rain environment.

the altitude of the satellite orbit is far greater than the rain height, and the size of the ground receiving antenna is far smaller than that of the rain area.

Based on the assumption mentioned above, we can consider an arbitrary polarization plane wave incident upon a semi-infinite medium containing a random distribution of many raindrops. In the coordinate axes xyz (see Figure 1 and Figure 2), the unit vector of incidence direction is $\hat{i}_0$, the field $\vec{u}(\vec{r}) = [u_H(\vec{r}) \quad u_V(\vec{r})]^T$ at $\vec{r} = (0, 0, L)$ consists of the average or coherent field $\langle \vec{u}(\vec{r}) \rangle = [\langle u_H(\vec{r}) \rangle \quad \langle u_V(\vec{r}) \rangle]^T$ and the fluctuation field or incoherent field $\vec{u}_f(\vec{r}) = [u_{f\_H}(\vec{r}) \quad u_{f\_V}(\vec{r})]^T$, where the subscripts H and V respectively denote the horizontal polarization component and the vertical polarization component. $\vec{u}(\vec{r})$ can be written as (1) [48]

$$\vec{u}(\vec{r}) = \langle \vec{u}(\vec{r}) \rangle + \vec{u}_f(\vec{r}) \tag{1}$$

And, the total intensity $I_t(\vec{r})$ of the receiving antenna at $\vec{r} = (0, 0, L)$ is presented as:

$$I_t(\vec{r}) = I_c(\vec{r}) + I_f(\vec{r}) \tag{2}$$

where, $I_c(\vec{r})$ is the coherent intensity, and $I_f(\vec{r})$ is the incoherent intensity.

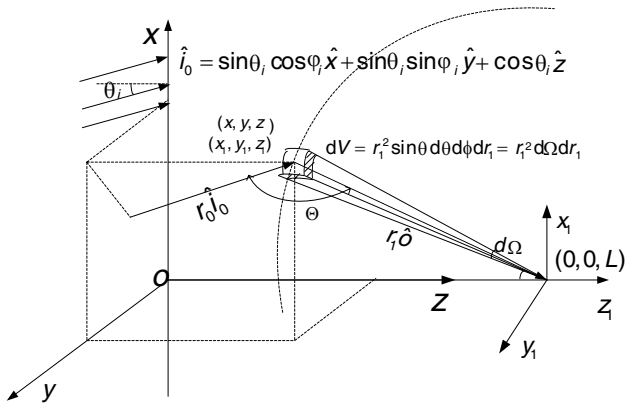

Figure 2. A plane wave incident on a semi-infinite medium containing a random distribution of many raindrops.

It is reasonable to evaluate the rain-induced propagation and scattering effects with the first-order multiple scattering approximation theory [48]. $\vec{u}_f(\vec{r})$ is a sum of the scattered fields from all the raindrops in the range $0 < z < L$, neglecting the backscattering contribution from

the region $z > L$, and $I_f(\vec{r})$ is a sum of the scattered intensity from all the raindrops in the range $0 < z < L$ [48].

According to the first-order multiple scattering approximation theory, the average or coherent field and the coherent intensity can be obtained by [48]

$$\left\langle u_{H(V)}(\vec{r})\right\rangle = u_{0\_H(V)} \exp(ikL/\cos\theta_i - \tau_{c\_H(V)}/2) \tag{3}$$

$$I_c = u_{0\_H}^2 \exp(-\tau_{c\_H}) + u_{0\_V}^2 \exp(-\tau_{c\_V}) \tag{4}$$

where, θ_i is the angle between the unit vector $\hat{i}_0$ and the axis z, $u_{0\_H(V)}$ the amplitude of the horizontal polarization component (the vertical polarization component) of the incident wave on the rain area, and $k = 2\pi/\lambda$ the wave number. In Equations (3) and (4), $\tau_{c\_H(V)}$ is the optical distance of the horizontal polarization wave (the vertical polarization wave), which is written as

$$\tau_{c\_H(V)} = \int_{D_{\min}}^{D_{\max}} \int_0^{L/\cos\theta_i} N(D)\sigma_{t\_H(V)}(D)\mathrm{d}r\mathrm{d}D = \rho \left\langle \sigma_{t\_H(V)} \right\rangle L/\cos\theta_i \tag{5}$$

where, $N(D)$ denotes raindrop size distribution function, and $\sigma_{t\_H(V)}(D)$ denotes the extinction cross section of the raindrop with the diameter D illuminated by the horizontal polarization wave (the vertical polarization wave), θ_i is the angle between the unit vector $\hat{i}_0$ and the axis z, ρ and $\langle\sigma_{t\_H(V)}\rangle$ are respectively denoted as [48, 49]

$$\rho = \int_{D_{\min}}^{D_{\max}} N(D)\mathrm{d}D \tag{6}$$

$$\left\langle \sigma_{t\_H(V)} \right\rangle = \frac{1}{\rho} \int_{D_{\min}}^{D_{\max}} N(D)\sigma_{t\_H(V)}(D)\mathrm{d}D \tag{7}$$

The coherent intensity is a constant value and can be readily calculated by (4) for an incidence direction. Therefore, the coherent intensity has little contribution to the angle distribution of the received intensity $I_t(\vec{r})$. And the angle distribution of the coherent intensity $I_c(\hat{i})$ can be written as

$$I_{c\_\vec{r}}\left(\hat{i}\right) = I_c \delta\left(\hat{i} - \hat{i}_0\right) \tag{8}$$

where, $\hat{i}$ is the concerned arriving direction in the coordinate axes xyz. In what follows, we will deduce the angle distribution of the incoherent intensity.

As mentioned before, $\vec{u}_f(\vec{r})$ is a sum of the scattered fields from all the raindrops in the range $0 < z < L$, and $I_f(\vec{r})$

is a sum of the scattered intensity from all the raindrops in the range $0 < z < L$. Let us first consider the scattering field $\vec{u}_f(D,\vec{r}) = [u_{f\_H}(D,\vec{r})\, u_{f\_V}(D,\vec{r})]^T$ at $\vec{r} = (0,0,L)$ from a single raindrop with the diameter D in $\mathrm{d}V$ located at (x,y,z) in the coordinate axes xyz. According to the scattering theory and the first order multiple scattering approximation theory, $\vec{u}_f(D,\vec{r}) = [u_{f\_H}(D,\vec{r})\, u_{f\_V}(D,\vec{r})]^T$ can be written as [48, 49]

$$\begin{bmatrix} u_{f\_H}(D,\vec{r}) \\ u_{f\_V}(D,\vec{r}) \end{bmatrix} = \begin{bmatrix} \frac{\exp(ikr_1)}{r_1}\Big[f_{11}\left(D,\hat{i}_0,\hat{o}\right) u'_{0\_H} \exp\left(-\tau_{1\_H}/2\right) \\ \quad +f_{12}\left(D,\hat{i}_0,\hat{o}\right) u'_{0\_V} \exp(-\tau_{1\_V}/2)\Big] \\ \frac{\exp(ikr_1)}{r_1}\Big[f_{21}\left(D,\hat{i}_0,\hat{o}\right) u'_{0\_H} \exp\left(-\tau_{1\_H}/2\right) \\ +f_{22}\left(D,\hat{i}_0,\hat{o}\right) u'_{0\_V} \exp(-\tau_{1\_V}/2)\Big] \end{bmatrix} \tag{9}$$

In Equation (9), u'_{0_H} and u'_{0_V} are the amplitude of the horizontal polarization component and the vertical polarization component of the incident wave on $\mathrm{d}V$, respectively; f_{11}, f_{12}, f_{21} and f_{22} are the elements of the scattering amplitude function matrix for the raindrop with the diameter D, which are the functions of scattering angle Θ ($\cos\Theta = \hat{i}_0 \cdot \hat{o}$), and are related to the scattering functions S_1, S_2, S_3 and S_4 used by Van de Hulst and in Mie solution for a sphere [48, 50]; $\hat{o}$ is the unit vector of a scattering direction in the coordinate axes xyz. r_1 is the distance from $\mathrm{d}V$ to $(0,0,L)$. u'_{0_H} and u'_{0_V} are given as (see Figure 2)

$$\begin{aligned} u'_{0\_H(V)} &= u_{0\_H(V)} \exp(ikr_0 - \tau_{0\_H(V)}/2) \\ &= u_{0\_H(V)} \exp\left(ik\frac{L - r_1\cos\theta}{\cos\theta_i} - \tau_{0\_H(V)}/2\right) \end{aligned} \tag{10}$$

where, $\tau_{0\_H(V)}$ is given as

$$\tau_{0\_H(V)} = \rho\langle\sigma_{t\_H(V)}\rangle(L - r_1\cos\theta)/\cos\theta_i \tag{11}$$

In Equations (10) and (11), θ is the angle between the unit vector $\hat{o}$ and the axis z.

$\tau_{1\_H(V)}$, in Equation (9), is written as

$$\tau_{1\_H(V)} = \rho\langle\sigma_{t\_H(V)}\rangle r_1 \tag{12}$$

f_{11}, f_{12}, f_{21} and f_{22} are presented as [48, 51]

$$\begin{aligned} f_{11} &= \frac{i}{k}S_1(D,\cos\Theta) \quad f_{12} = \frac{i}{k}S_4(D,\cos\Theta) \\ f_{21} &= \frac{i}{k}S_3(D,\cos\Theta) \quad f_{22} = \frac{i}{k}S_2(D,\cos\Theta) \end{aligned} \tag{13}$$

$\sigma_{t\_H(V)}(D)$ can be written as

$$\sigma_{t\_H}(D) = \frac{4\pi}{k}\mathrm{Im}\left[f_{11}\Big(D,\hat{i}_0,\hat{i}_0\Big)\right] \quad \sigma_{t\_V} = \frac{4\pi}{k}\mathrm{Im}\left[f_{22}\Big(D,\hat{i}_0,\hat{i}_0\Big)\right] \quad (14)$$

Note that if the particle is spherically symmetric, $f_{12} = f_{21} = 0$, which is approximatively suitable for raindrop [48]. Therefore, (9) is simplified as

$$\begin{bmatrix} u_{f\_H}(D,\vec{r}) \\ u_{f\_V}(D,\vec{r}) \end{bmatrix} = \begin{bmatrix} \frac{\exp(ikr_1)}{r_1} f_{11}(D,\cos\Theta) u'_{0\_H} \exp(-\tau_{1\_H}/2) \\ \frac{\exp(ikr_1)}{r_1} f_{22}(D,\cos\Theta) u'_{0\_V} \exp(-\tau_{1\_V}/2) \end{bmatrix} \quad (15)$$

where, $\cos\Theta = \hat{i}_0 \cdot \hat{o}$. In the coordinate axes xyz, $\hat{i}_0$ and $\hat{o}$ can be written as

$$\hat{i}_0 = \sin\theta_i\cos\phi_i\hat{x} + \sin\theta_i\sin\phi_i\hat{y} + \cos\theta_i\hat{z} \quad (16)$$

$$\hat{o} = \sin\theta\cos\phi\hat{x} + \sin\theta\sin\phi\hat{y} + \cos\theta\hat{z} \quad (17)$$

In Equations (16) and (17), θ_i is the angle between the unit vector $\hat{i}_0$ and the axis z, φ_i is the angle between the projection of $\hat{i}_0$ in the plane xy and the axis x, and θ is the angle between the unit vector $\hat{o}$ and the axis z, φ is the angle between the projection of $\hat{o}$ in the plane xy and the axis x. Therefore, $\cos\Theta = \hat{i}_0 \cdot \hat{o}$ is derived as

$$\cos\Theta = \sin\theta\cos\varphi\sin\theta_i\cos\varphi_i + \sin\theta\sin\varphi\sin\theta_i\sin\varphi_i + \cos\theta\cos\theta_i \quad (18)$$

Consequently, the received incoherent intensity $\mathrm{d}I_f(\vec{r})$ from the raindrops in $\mathrm{d}V$ can be presented as

$$\begin{aligned}\mathrm{d}I_f(\vec{r}) &= \int_{D_{\min}}^{D_{\max}} \left[\left|u_{f\_H}(D,\vec{r})\right|^2 + \left|u_{f\_V}(D,\vec{r})\right|^2\right] N(D)\mathrm{d}V\mathrm{d}D \\ &= \int_{D_{\min}}^{D_{\max}} \frac{|f_{11}(D,\cos\Theta)|^2}{(r_1)^2}(u_{0\_H})^2\exp(-\tau_{1\_H}-\tau_{0\_H})N(D)\mathrm{d}V\mathrm{d}D \\ &\quad + \int_{D_{\min}}^{D_{\max}} \frac{|f_{22}(D,\cos\Theta)|^2}{(r_1)^2}(u_{0\_V})^2\exp(-\tau_{1\_V}-\tau_{0\_V})N(D)\mathrm{d}V\mathrm{d}D \quad (19)\end{aligned}$$

Define $\langle|f_{11(22)}(\cos\Theta)|^2\rangle$ as [48, 52]

$$\left\langle\left|f_{11(22)}(\cos\Theta)\right|^2\right\rangle = \frac{1}{\rho}\int_{D_{\min}}^{D_{\max}} N(D)\left|f_{11(22)}(D,\cos\Theta)\right|^2\mathrm{d}D \quad (20)$$

Equation (19) can be written as

$$\begin{aligned}\mathrm{d}I_f(\vec{r}) &= \frac{\rho}{(r_1)^2}\Big\{\left\langle|f_{11}(\cos\Theta)|^2\right\rangle(u_{0\_H})^2\exp(-\tau_{1\_H}-\tau_{0\_H}) \\ &\quad + \left\langle|f_{22}(\cos\Theta)|^2\right\rangle(u_{0\_V})^2\exp(-\tau_{1\_V}-\tau_{0\_V})\Big\}\mathrm{d}V \quad (21)\end{aligned}$$

For convenience, analyse Equation (21) in the new coordinate axes $x_1y_1z_1$, whose origin is the point $(0, 0, L)$ in the coordinate axes xyz (see Figure 2). In the coordinate axes $x_1y_1z_1$, $\mathrm{d}V$ is located at (x_1, y_1, z_1), which is also (r_1, θ, φ), so $\mathrm{d}V$ can be written as

$$\mathrm{d}V = r_1^2 \sin\theta \mathrm{d}\theta \mathrm{d}\phi \mathrm{d}r_1 = r_1^2 \mathrm{d}\Omega \mathrm{d}r_1 \tag{22}$$

Define $I_{f\_\vec{r}}(\theta, \varphi)$ as

$$I_{f\_\vec{r}}(\theta, \varphi) = \int_0^R \frac{\mathrm{d}I_f(\vec{r})}{\mathrm{d}\Omega} r_1^2 \mathrm{d}r_1 \tag{23}$$

Equation (23) means the received incoherent intensity at $\vec{r} = (0, 0, L)$ coming from the direction of (θ, φ) in the coordinate $x_1y_1z_1$ also in the coordinate xyz, i.e., $I_{f\_\vec{r}}(\theta, \varphi)$ is the angle distribution function of the incoherent intensity. $I_{f\_\vec{r}}(\theta, \varphi)$ can be derived from Equations (21)–(23) as

$$\begin{aligned} I_{f\_\vec{r}}(\theta, \varphi) = \int_0^{L/\cos\theta} \frac{\rho}{(r_1)^2} \Big\{ \Big\langle |f_{11}(\cos\Theta)|^2 \Big\rangle (u_{0\_H})^2 \exp(-\tau_{1\_H} - \tau_{0\_H}) \\ + \Big\langle |f_{22}(\cos\Theta)|^2 \Big\rangle (u_{0\_V})^2 \exp(-\tau_{1\_V} - \tau_{0\_V}) \Big\} r_1^2 \mathrm{d}r_1 \end{aligned} \tag{24}$$

By using Equations (11), (12) and (18), Equation (24) can be simplified as

$$I_{f\_\vec{r}}(\mu, \varphi) = \begin{cases} \frac{\mu_i \rho}{(\mu_i - \mu)} \left[\Big\langle |f_{11}(\cos\Theta)|^2 \Big\rangle g_H + \Big\langle |f_{22}(\cos\Theta)|^2 \Big\rangle g_V \right] & \mu \neq \mu_i \\ \frac{\rho L}{\mu} \left[\Big\langle |f_{11}(\cos\Theta)|^2 \Big\rangle g_{1\_H} + \Big\langle |f_{22}(\cos\Theta)|^2 \Big\rangle g_{1\_V} \right] & \mu = \mu_i \end{cases} \tag{25}$$

In Equation (25)

$$\mu = \cos\theta \quad \mu_i = \cos\theta_i \tag{26}$$

$$g_{H(V)} = \frac{[u_{0\_H(V)}]^2 [\exp(-\gamma_{\_H(V)} L/\mu_i) - \exp(-\gamma_{\_H(V)} L/\mu)]}{\gamma_{\_H(V)}} \tag{27}$$

$$g_{1\_H(V)} = [u_{0\_H(V)}]^2 \exp[-\gamma_{H(V)} L/\mu_i] \tag{28}$$

where, $\gamma_{H(V)} = \rho \left\langle \sigma_{t\_H(V)} \right\rangle$. By the way, if a raindrop is regarded as an isotropic, homogeneous sphere, $\gamma_H = \gamma_V$, which is not well suitable for rain environment (especially in the case of a large rain rate). γ_H and γ_V can be calculated by the model given in ITU-R P.838 [53].

Rewrite (8) using μ and φ as

$$I_{c\_\vec{r}}(\mu, \varphi) = I_c \delta(\mu - \mu_i) \delta(\varphi - \varphi_i) \tag{29}$$

Now, the angle distribution $I_{t\_\vec{r}}(\mu, \varphi)$ can be given as

$$I_{t\_\vec{r}}(\mu, \varphi) = I_{c\_\vec{r}}(\mu, \varphi) + I_{f\_\vec{r}}(\mu, \varphi) \tag{30}$$

PAS $P_{\vec{r}}(\theta, \varphi)$ of the antenna located at $\vec{r} = (0, 0, L)$ can be given as

$$P_{\vec{r}}(\theta, \varphi) = I_{t\_\vec{r}}(\mu, \varphi) A(\theta, \varphi) m_P \tag{31}$$

where, m_P is the polarization mismatch factor and a real number between zero and one, which depends on the degree of match of the polarization state of the wave and the antenna [54], $A(\theta, \varphi)$ is the effective aperture in the direction (θ, φ), which can be calculated by

$$A(\theta, \varphi) = \frac{\lambda^2}{4\pi} G(\theta, \varphi) \tag{32}$$

where, λ is the wave length of the incident wave and $G(\theta, \varphi)$ the gain of the receiving antenna.

3. NUMERICAL RESULTS AND DISCUSSION

The model given in Section 2 is suitable for a practical downlink with an arbitrary polarization incident wave in an arbitrary incident direction in the coordinate axes similar to those in Figure 1 and Figure 2. The incident direction for a real downlink is determined

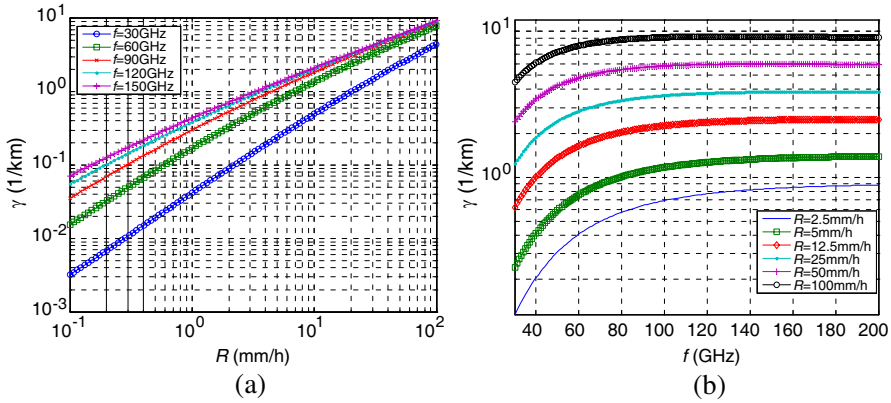

Figure 3. $\gamma = \gamma_H = \gamma_V$ varying with the rain rate and frequency, (a) shows $\gamma = \gamma_H = \gamma_V$ varying with the rain rate for the frequencies of 30 GHz, 60 GHz, 90 GHz, 120 GHz and 150 GHz, (b) shows $\gamma = \gamma_H = \gamma_V$ varying with the frequency for the rain rates of 2.5 mm/h, 5 mm/h, 12.5 mm/h, 25 mm/h, 50 mm/h and 100 mm/h.

by the link geometry structure. In this section, $\gamma_{H(V)} = \rho\left\langle\sigma_{t\_H(V)}\right\rangle$, $\langle|f_{11}(\cos\Theta)|^2\rangle$ (which is for horizontal polarization), $\langle|f_{22}(\cos\Theta)|^2\rangle$ (which is for vertical polarization), and the PAS are calculated and discussed by Mie method based on the Marshall-Palmer raindrop size distribution [55]. Note that PAS is analyzed under the conditions of $A(\theta,\varphi) = 1$, $m_P = 1$ and the intensity of incident wave is equal to 1.

Figure 3 is the results of $\gamma = \gamma_H = \gamma_V$ varying with the corresponding rain rate and frequency. Figure 4 gives the results of $\langle|f_{11}(\cos\Theta)|^2\rangle$ and $\langle|f_{22}(\cos\Theta)|^2\rangle$ varying with the scattering angle for different frequencies in different rain environments. Figure 5 gives a two-dimension PAS example of the vertical polarization incident wave

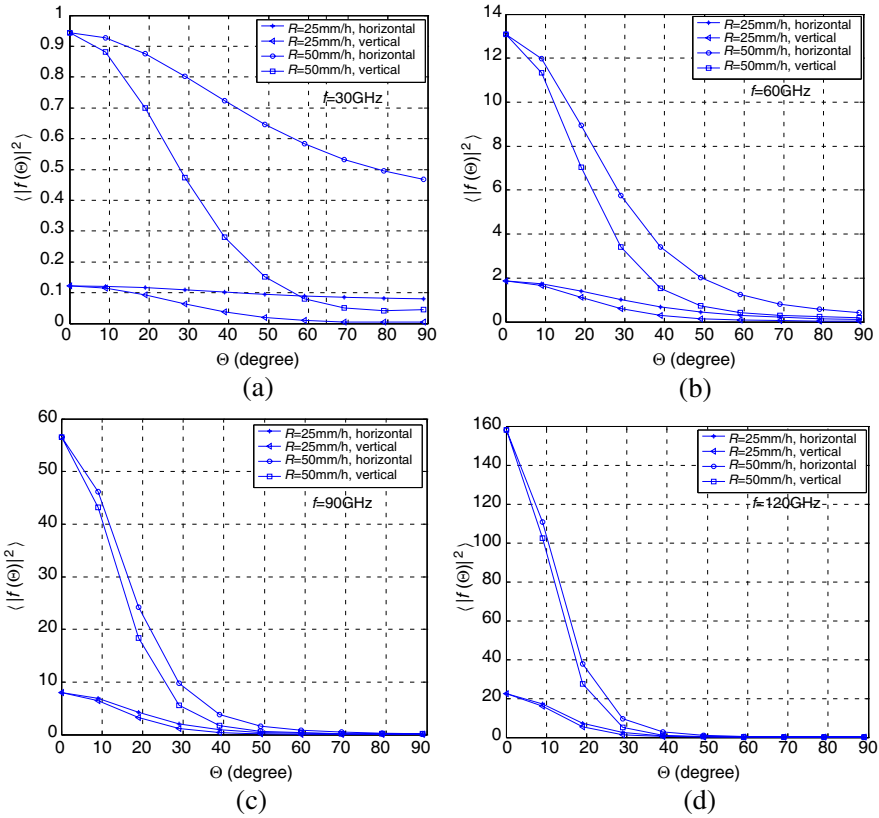

Figure 4. $\langle|f_{11}(\cos\Theta)|^2\rangle$ (see "horizontal" in these figures) and $\langle|f_{22}(\cos\Theta)|^2\rangle$ (see "vertical" in these figures) varying with the scattering angle for the frequencies of 30 GHz, 60 GHz, 90 GHz, and 120 GHz.

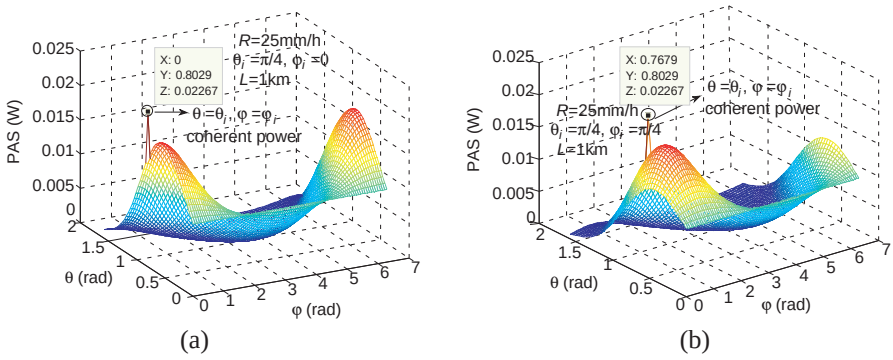

Figure 5. An example of the two-dimension PAS for the vertical polarization incident wave at 90 GHz for different incident directions.

at 90 GHz. Figure 6–Figure 8 show the one-dimension incoherent power varying with the rain height L, rain rate, and the frequency, the polarization and the incident angle of the incident wave.

Figure 3 shows that γ approximately increases linearly with the rain rate for the same frequency on log paper; γ increases with the frequency for the same rain rate, but γ is close to a constant value with frequency increasing, and the larger the rain rate is, the greater the constant value is.

It can be concluded from Figure 4 that $\langle|f_{11}(\cos\Theta)|^2\rangle$ and $\langle|f_{22}(\cos\Theta)|^2\rangle$ differently change with the scattering angle for different frequencies and rain rates. If $\Theta \neq 0$, $\langle|f_{11}(\cos\Theta)|^2\rangle$ is greater than $\langle|f_{22}(\cos\Theta)|^2\rangle$ for the same frequency and rain rate; for the same frequency, $\langle|f_{11}(\cos\Theta)|^2\rangle$ distinctly exceeds $\langle|f_{22}(\cos\Theta)|^2\rangle$ for the larger rain rate; for the same rain rate, $\langle|f_{11}(\cos\Theta)|^2\rangle$ distinctly exceeds $\langle|f_{22}(\cos\Theta)|^2\rangle$ for the lower frequency. If $\Theta = 0$, $\langle|f_{11}(\cos\Theta)|^2\rangle$ is equal to $\langle|f_{22}(\cos\Theta)|^2\rangle$ for the same frequency and rain rate; for the same frequency, the larger the rain rate is, the greater $\langle|f_{11}(\cos\Theta)|^2\rangle$ and $\langle|f_{22}(\cos\Theta)|^2\rangle$ are; for the same rain rate, the higher the frequency is, the greater $\langle|f_{11}(\cos\Theta)|^2\rangle$ and $\langle|f_{22}(\cos\Theta)|^2\rangle$ are.

Figure 5 shows that the PAS is mainly affected by the incoherent intensity or the incoherent power, which is coming from different directions. Therefore, AS (angle spread) is caused by the incoherent power. Although the exhibited results are for the vertical polarization incident wave at 90 GHz, the patterns for horizontal polarization incident wave and other frequencies are similar. Consequently, Figure 6–Figure 8 mainly discuss the one-dimension incoherent power angle distribution changing with rain environment parameters, and the frequency, the polarization and the incident angle of the incident wave.

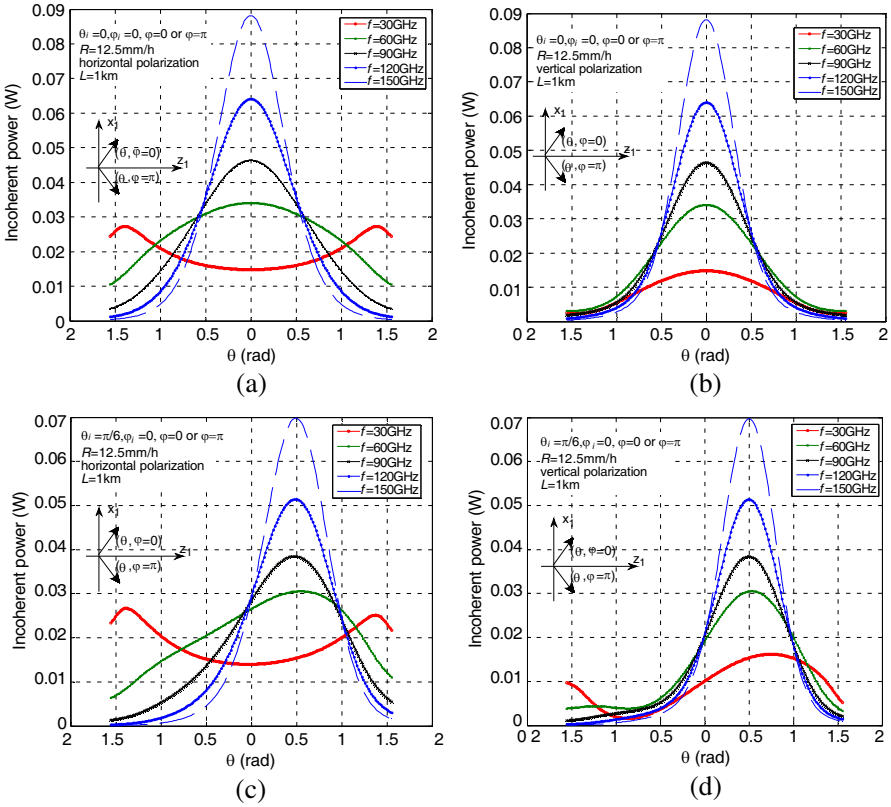

Figure 6. The incoherent power angle distribution for the horizontal and the vertical polarization at 30 GHz, 60 GHz, 90 GHz, 120 GHz and 150 GHz. Note that the left part from $\theta = 0$ of these figures is the result under the condition of $\varphi = \pi$ and the right part $\varphi = 0$.

It can be concluded from Figure 6 that if the rain environment parameters and the incident wave characteristics are given, the incoherent power focuses on the forward scattering direction (namely "forward scattering character" in this paper) more obviously for higher frequency, which also means the incoherent power has a narrow angle distribution. Figure 6 also shows that the "forward scattering character" can be completely destroyed at the lower frequency if the other conditions are the same.

Figure 7 shows that a larger rain rate or rain height can make the "forward scattering character" more obvious for the same characteristics of the incident wave for the lower frequency. Figure 8

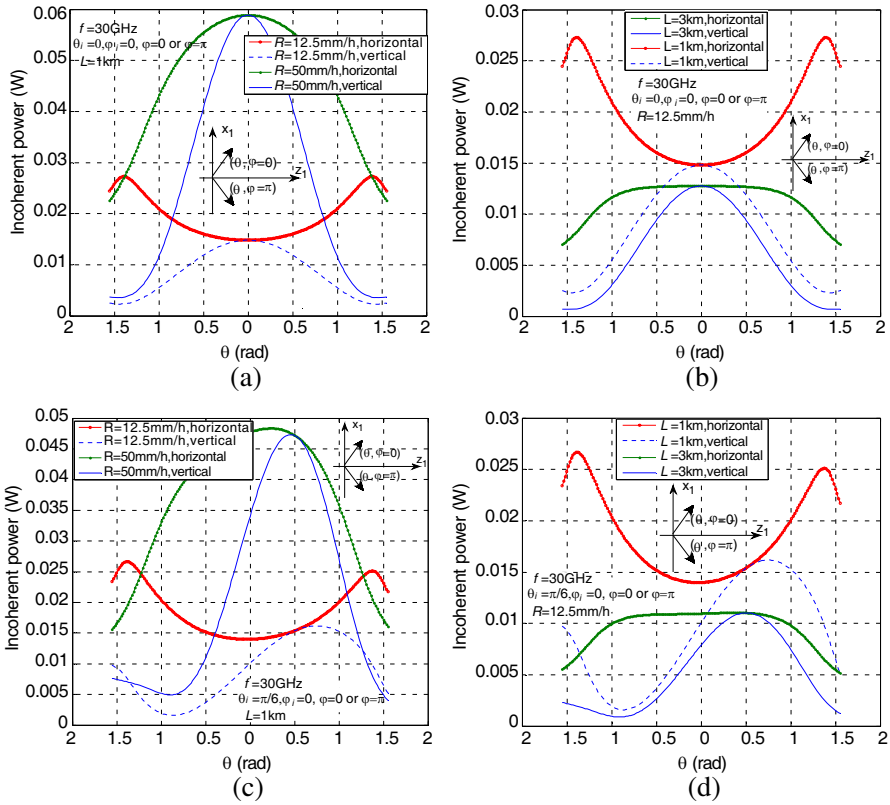

Figure 7. The incoherent power angle distribution for the horizontal and the vertical polarization at 30 GHz. Note that the left part from $\theta = 0$ of these figures is the result under the condition of $\varphi = \pi$ and the right part $\varphi = 0$.

shows that the peak of the incoherent power is determined by the rain rate and rain height for the same incident wave characteristics.

As shown in Figure 6–Figure 8, the incoherent power angle distribution has complicated relationship with the rain environment parameters (such as rain rate, rain height) and the incident wave characteristics (such as frequency, polarization, and incident angle). It can be concluded that the raindrop size distribution also has impacts on the result of PAS. So, it is necessary to calculate the PAS under a specific link and the rain environment parameters for investigating MMW MIMO channel characteristics.

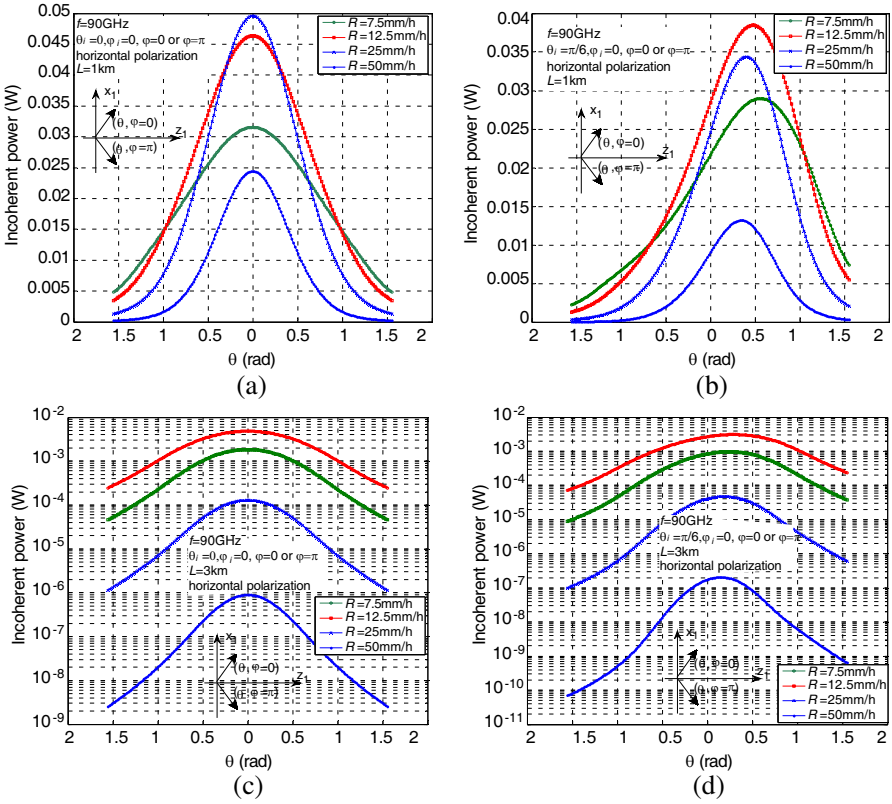

Figure 8. The incoherent power angle distribution for the horizontal polarization at 90 GHz. Note that the left part from $\theta = 0$ of these figures is the result under the condition of $\varphi = \pi$ and the right part $\varphi = 0$.

4. CONCLUSIONS

We have investigated the power angle spectrum (PAS) of the satellite communication downlink in rain environment at millimeter-wave bands. The coherent intensity is discussed according to the first-order multiple scattering approximation theory, and the two-dimension angle distribution expression of the incoherent intensity of the ground receiving antenna in rain environment is deduced in detail. The calculation model of PAS is given based on the coherent intensity and the incoherent intensity angle distribution model. The model given in this paper is suitable for a practical downlink with an arbitrary polarization incident wave in an arbitrary incident direction in the coordination similar to those in Figure 1 and Figure 2.

In this paper, $\gamma_{H(V)} = \rho \left\langle \sigma_{t\_H(V)} \right\rangle$, $\langle |f_{11}(\cos\Theta)|^2 \rangle$, $\langle |f_{22}(\cos\Theta)|^2 \rangle$, and the PAS are calculated and discussed by Mie method based on the Marshall-Palmer raindrop size distribution. Note that PAS is analyzed under the conditions of $A(\theta, \varphi) = 1$, $m_P = 1$ and the intensity of incident wave is equal to 1. It can be concluded based on the simulation results in this paper that PAS has complicated relationship with the rain environment parameters (such as rain rate, rain height, and raindrop size distribution) and the incident wave characteristics (such as frequency, polarization, and incident angle). Therefore, it is necessary to calculate PAS under a specific link and the environment parameters using the model given in this paper for investigating MMW MIMO channel characteristics.

ACKNOWLEDGMENT

The authors would like to thank the National Natural Science Foundation of China under Grant No. 61001065, and the Fundamental Research Funds for the Central Universities for financial support of this work.

REFERENCES

1. Gong, S. H., "Study on some problems for radio wave propagating and scattering through troposphere," Ph.D. Dissertation, Department of Science, Xidian University, Xi'an, China, 2008.
2. Arapoglou, P. D., K. Liolis, M. Bertinelli, et al., "MIMO over satellite, a review," *IEEE Communications Surveys & Tutorials First Quarter*, Vol. 13, No. 1, 27–51, 2011.
3. Paulraj, A. J., D. A. Gore, R. U. Nabar, et al., "An overview of MIMO communications — A key to gigabit wireless," *Proceedings of the IEEE,* Vol. 92, No. 2, 198–218, 2004.
4. Huang, K. C. and Z. C. Wang, *Millimeter Wave Communication Systems,* 133–162, John Wiley & Sons, 2011.
5. Pi, Z. Y. and F. Khan, "A millimeter-wave massive MIMO system for next generation mobile broadband," *Signals, Systems and Computers (ASILOMAR),* 693–698, 2012.
6. Suzuki, S., T. Nakagawa, H. Furuta, et al., "Evaluation of millimeter-wave MIMO-OFDM transmission performance in a TV studio," *IEEE Asia-Pacific Microwave Conference, APMC*, 843–846, 2006.

7. Madhow, U., "MultiGigabit millimeter wave communication: System concepts and challenges," *IEEE Information Theory and Applications Workshop,* 193–196, 2008.
8. Moraitis, N. and P. Constantinou, "Indoor channel capacity evaluation utilizing ULA and URA antennas in the millimeter wave band," *IEEE 18th International Symposium on Personal, Indoor and Mobile Radio Communications, PIMRC*, 1–5, 2007.
9. Torkildson, E., C. Sheldon, U. Madhow, et al., "Millimeter-wave spatial multiplexing in an indoor environment," *IEEE Globecom Workshops*, 1–6, 2009.
10. Ranvier, S., C. Icheln, and P. Vainikainen, "Measurement-based mutual information analysis of MIMO antenna selection in the 60-GHz band," *IEEE Antennas and Wireless Propagation Letters*, Vol. 8, 686–689, 2009.
11. Sheldon, C., E. Torkildson, M. Seo, et al., "A 60 GHz line-of-sight 2×2 MIMO link operating at 1.2 Gbps," *IEEE Antennas and Propagation Society International Symposium, AP-S*, 1–4, 2008.
12. Sheldon, C., M. Seo, E. Torkildson, et al., "Four-channel spatial multiplexing over a millimeter-wave line-of-sight link," *IEEE MTT-S International Microwave Symposium Digest, MTT'09*, 389–392, 2009.
13. Manojna, D. S., S. Kirthiga, and M. Jayakumar, "Study of 2×2 spatial multiplexed system in 60 GHz indoor environment," *International Conference on Process Automation, Control and Computing*, 1–5, 2011.
14. Torkildson, E., U. Madhow, and M. Rodwell, "Indoor millimeter wave MIMO: Feasibility and performance," *IEEE Trans. on Wireless Communications*, Vol. 10, 4150–4160, 2011.
15. Sheldon, C., E. Torkildson, M. Seo, et al., "Spatial multiplexing over a line-of-sight millimeter-wave MIMO link: A two-channel hardware demonstration at 1.2 Gbps over 41 m range," *European Wireless Technology Conference*, 198–201, 2008.
16. Moraitis, N., D. Vouyioukas, V. Milas, et al., "Outdoor capacity study utilizing multiple element antennas at the millimeter wave band," *IEEE International Conference on Wireless and Mobile Computing, Networking And Communications — WiMob*, 2–7, 2007.
17. Ranvier, S., S. Geng, and P. Vainikainen, "Mm-wave MIMO systems for high data-rate mobile communications," *1st International Conference on Wireless Communication, Vehicular Technology, Information Theory and Aerospace and Electronic Systems Technology — Wireless VITAE*, 142–146, 2009.

18. Xia, P. F., H. N. Niu, J. Oh, et al., "Practical antenna training for millimeter wave MIMO communication," *IEEE Vehicular Technology Conference, (VTC Spring)*, 1–5, 2008.
19. Toda, A. P., F. de Flaviis, and J. Castaneda, "60 GHz waveguide array design for MIMO channel characterization," *IEEE International Conference on Ultra-wideband ICUWB*, 12–16, 2009.
20. Ranvier, S., J. Kivinen, and P. Vainikainen, "Millimeter-wave MIMO radio channel sounder," *IEEE Trans. on Instrumentation and Measurement*, Vol. 56, 1018–1024, 2007.
21. Palaskas, Y., A. Ravi, and S. Pellerano, "MIMO techniques for high data rate radio communications," *IEEE Custom Intergrated Circuits Conference (CICC)*, 141–148, 2008.
22. Kivinen, J., "60-GHz wideband radio channel sounder," *IEEE Trans. on Instrumentation and Measurement*, Vol. 56, 1831–1838, 2007.
23. Pollok, A., W. G. Cowley, and I. D. Holland, "Multiple-input multiple-output options for 60 GHz line-of-sight channels," *Communications Theory Workshop (ASCTW)*, 101–106, 2008.
24. Peter, M., W. Keusgen, and J. Luo, "A survey on 60 GHz broadband communication: Capability, applications and system design," *Microwave Integrated Circuit Conference European*, 1–4, 2008.
25. Nsenga, J., W. Van Thillo, F. Horlin, et al., "Joint transmit and receive analog beamforming in 60 GHz MIMO multipath channels," *IEEE International Conference on Communications*, 1–5, 2009.
26. Torkildson, E., H. Zhang, and U. Madhow, "Channel modeling for millimeter wave MIMO," *Information Theory and Applications Workshop (ITA)*, 1–8, 2010.
27. Zhang, H., S. Venkateswaran, and U. Madhow, "Channel modeling and MIMO capacity for outdoor millimeter wave links," *IEEE Wireless Communications and Networking Conference (WCNC)*, 1–6, 2010.
28. Lee, S. J., M. G. Kyeong, and W. Y. Lee, "Capacity analysis of MIMO channel with line-of-sight and reflected paths for millimeter-wave communication," *International Conference on Signal Processing and Communication Systems (ICSPCS)*, 1–5, 2010.
29. Ahmadi-Shokouh, J., R. Rafi, A. Taeb, et al., "Real-time Millimeter-Wave MIMO channel measurements," *2012 IEEE*

Antennas and Propagation Society International Symposium (APSURSI), 1–2, 2012.

30. Ayach, R. W. H., J. S. Abu-Surra, et al., "The capacity optimality of beam steering in large millimeter wave MIMO systems," *The 13th IEEE International Workshop on Signal Processing Advances in Wireless Communications (SPAWC)*, 100–104, 2012,
31. Kolani, I. and J. Zhang, "Millimeter wave for MIMO small antenna systems and for mobile handset," *2011 International Conference on Computer Science and Network Technology (ICCSNT)*, 150–153, 2011.
32. Ayach, O. E., R. W. Heath, J. S. Abu-Surra, et al., "Low complexity precoding for large millimeter wave MIMO systems," *IEEE International Conference on Communications (ICC)*, 3724–3729, 2012.
33. Lee, S. J., W. Lee, S. E. Hong, et al., "Performance evaluation of beamformed spatial multiplexing transmission in millimeter-wave communication channels," *IEEE 77th Vehicular Technology Conference (VTC Fall)*, 1–5, 2012.
34. Brady, J., N. Behdad, and A. M. Sayeed, "Beamspace MIMO for millimeter-wave communications: System architecture, modeling, analysis, and measurements," *IEEE Trans. on Antennas and Propagation*, Vol. 61, 3814–3827, 2013.
35. Liolis, K. P. and A. D. Panagopoulos, "On the applicability of MIMO principle to 10–66 GHz BFWA networks: Capacity enhancement through spatial multiplexing and interference reduction through selection diversity," *IEEE Trans. on Communications*, Vol. 57, 530–541, 2009.
36. Ishimaru, A., J. Ritcey, S. Jaruwatanadilok, et al., "A MIMO propagation channel model in a random medium," *Antennas and Propagation Society International Symposium*, 1341–1344, 2007.
37. Liolis, K. P. and B. D. Rao, "Application of MIMO theory to the analysis of broadband fixed wireless access diversity systems above 10 GHz," *Antennas and Propagation Society International Symposium*, 145–148, 2006.
38. Ishimaru, A., S. Jaruwatanadilok, J. A. Ritcey, et al., "A MIMO propagation channel model in a random medium," *IEEE Trans. on Antennas and Propagation*, Vol. 58, 178–186, 2010.
39. Frigyes, I. and P. Horvith, "Mitigation of rain-induced fading: Route diversity vs rout-time coding," *IEE Twelfth International Conference on Antennas and Propagation (ICAP)*, 292–295, 2003.

40. Oh, C. I., S. H. Choit, D. I. Chang, et al., "Analysis of the rain fading channel and the system applying MIMO," *International Symposium on Communications and Information Technologies (ISCIT)*, 507–510, 2006.
41. Schwarz, R. T., A. Knopp, and B. Lankl, "The channel capacity of MIMO satellite links in a fading environment: A probabilistic analysis," *International Workshop on Satellite and Space Communications 2009*, 78–82, 2009.
42. Liolis, K. P., A. D. Panagopoulos, and P. G. Cottis, "Bit-error outage over SIMO spatially correlated rain-fading channels," *IEEE Antennas and Propagation Magazine*, Vol. 53, 204–209, 2011.
43. Liolis, K. P., A. D. Panagopoulos, and P. G. Cottis, "Multi-satellite MIMO communications at Ku-band and above: Investigations on spatial multiplexing for capacity improvement and selection diversity for interference mitigation," *EURASIP Journal on Wireless Communications and Networking*, Vol. 2007, 1–11, 2007.
44. Lee, W., "Effects on correlation between two mobile radio base-station antennas," *IEEE Trans. on Communications,* Vol. 21, No. 11, 1214–1224, 1973.
45. Salz, J. and J. H. Winters, "Effect of fading correlation on adaptive arrays in digital mobile radio," *IEEE Trans. on Vehicular Technology*, Vol. 43, No. 4, 1049–1057, 1994.
46. Asztély, D., "On antenna arrays in mobile communication systems: Fast fading and GSM base station receiver algorithms," Ph.D. Dissertation, Royal Institute of Technology, Stockholm, Sweden, IR-S3-SB-9611, 1996.
47. Pedersen, K., I., P. E. Mogensen, and B. H. Fleury, "Spatial channel characteristics in outdoor environments and their impact on BS antenna system performance," *IEEE 48th Vehicular Technology Conference*, Vol. 2, 1998.
48. Ishimaru, A., *Wave Propagation and Scattering in Random Media*, Vol. 2, Academic Press, New York, 1978.
49. Setijadi, E., A. Matsushima, N. Tanaka, and G. Hendrantoro, "Effect of temperature and multiple scattering on rain attenuation of electromagnetic waves by a simple spherical model," *Progress In Electromagnetics Research*, Vol. 99, 339–354, 2009.
50. Van de Hulst, H. C., *Light Scattering: By Small Particles*, Courier Dover Publications, 1957.

51. Ishimaru, A. and L. T. C. Rudolf, "Multiple scattering effects on wave propagation due to rain," *Annales des Télécommunications*, Vol. 35. Nos. 11–12, 373–379, Springer-Verlag, 1980.
52. Huang, J. Y., S. H. Gong, and F. Wang, "Optimal scattering polarization characteristic for cylinder target in rain at millimeter wave band," *Progress In Electromagnetics Research*, Vol. 55, 241–248, 2005.
53. ITU-R Recommendation P.311-13, "Specific attenuation model for rain for use in prediction methods," International Telecommunication Union, Geneva, 2005.
54. Zhang, B. Q., S. H. Gong, W. Y. Wang, et al., "Study on the characteristics of rain-induced polarization mismatch factor at Ka bands," *Hans Journal of Wireless Communications*, Vol. 2, No. 1, 1–6, 2012.
55. Battan, L. J., *Radar Observation of the Atmosphere*, 41, University of Chicago Press, Chicago, Illinois, 1973.